Composites Part B 284 (2024) 111676

Contents lists available at ScienceDirect

Composites Part B

journal homepage: www.elsevier.com/locate/compositesb

CF/PEEK skins assembly by induction welding for thermoplastic composite sandwich panels

Romain G. Martin [a], Christer Johansson [b], Jason R. Tavares [c], Martine Dubé [a,*]

[a] CREPEC, Mechanical Engineering, École de technologie supérieure (ÉTS), Montréal, QC, Canada
[b] RISE Research Institutes of Sweden, Göteborg, Sweden
[c] CREPEC, Chemical Engineering, Polytechnique Montréal, Montréal, QC, Canada

ARTICLE INFO

Handling Editor: Uday Vaidya

Keywords:
Carbon fibre
Thermoplastic resin
Honeycomb
Mechanical properties
Induction welding

ABSTRACT

A method to assemble sandwich panels made of carbon fibre reinforced poly-ether-ether-ketone (CF/PEEK) facesheets and 3D-printed poly-ether-imide (PEI) honeycomb cores using induction welding is presented. Induction heating patterns inside CF/PEEK laminates of variable dimensions are first evaluated with a thermal camera and compared to a COMSOL Multiphysics model. Sandwich samples are then prepared by vacuum-assisted continuous induction welding under parameters selected from the modelling effort. Joining of sandwich panels made of CF/PEEK facesheets by induction welding under vacuum is demonstrated. Facesheets do not deconsolidate in the process and core crushing is avoided. Flatwise skin/core strength of the welded samples reaches up to 7 MPa, above reported performance for thermoset or thermoplastic composite sandwich panels.

1. Introduction

Thermoplastic composites are gaining traction in the aerospace and automotive fields due to their unlimited shelf life, their weldability, and their recyclability [1]. Welding in particular is increasingly used in various fields to assemble thermoplastic composite parts. Various welding methods exist, relying on thermal, friction or electromagnetic mechanisms to generate heat at the joining interface [2]. Amongst these, ultrasonic welding, resistance welding and induction welding are the most used methods and are already implemented in industry [3]. They all present advantages and limitations, which makes them complementary. In the present study, the focus is placed on induction welding as a joining technique to fabricate thermoplastic composite sandwich panels.

1.1. Induction welding

Induction welding relies on the application of an alternating magnetic field on the joining interface to melt or soften the surrounding thermoplastic polymer. Heat can be generated at the interface by two different mechanisms: induced eddy currents in electrically-conductive materials ([2,4,5]), or hysteresis losses in magnetic materials ([6–8]). When needed, a heating element called a susceptor can be placed at the interface to localise the heat generation. This is required when welding non-conductive composites, such as those made of glass or natural fibres, which do not possess the ability to heat up by induction. Due to their good electrical conductivity, carbon fibre reinforced thermoplastic composites can be welded without using a susceptor, in a process known as susceptor-less welding ([5,9–11]). As an alternating magnetic field is applied to the laminate, eddy currents are induced in the carbon fibres, which heat up due to the Joule effect. Three main mechanisms are responsible for the heat dissipation inside the laminate ([4,5,12,13]). First, the heat is generated by the Joule effect as current circulates in the fibres. Secondly, at the intersection of fibres – typically between two non-parallel plies in laminates composed of unidirectional layers, or at the junctions of fibres in woven fabrics – heat is generated by contact resistance or, thirdly, by dielectric heating when a thin layer of polymer stands in between the two fibre tows. Those mechanisms all contribute to the induction heating of laminates.

There is one important drawback to using the susceptor-less method: when eddy currents are induced in an electrically-conductive material, the formed current paths are loops. When the induction coil approaches the edges of the material, these loops are compressed, locally increasing the current density and inducing high heat generation at the edges (edge effect) ([4,14]). This phenomenon, schematized in Fig. 1, causes inhomogeneous heating at the joining interface and must be minimized.

* Corresponding author.
E-mail address: martine.dube@etsmtl.ca (M. Dubé).

https://doi.org/10.1016/j.compositesb.2024.111676
Received 24 April 2024; Received in revised form 7 June 2024; Accepted 30 June 2024
Available online 2 July 2024

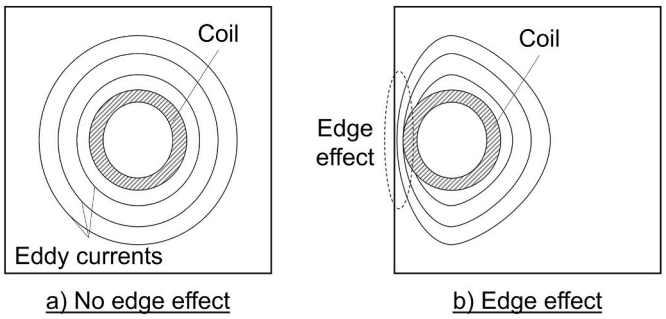

Fig. 1. Scheme of eddy currents distribution in an electrically-conductive material (a) without and (b) with edge effects due to induced eddy current loops concentration.

Different propositions have been made to reduce this effect, such as for example placing a conductive bypass material at the edges of the parts [15].

1.2. Modelling of laminate heating by induction

Understanding and predicting the temperature distribution in a laminate to be welded is critical to ensure the good quality of the weld. As explained, different mechanisms impact heat generation, and variation of local parameters such as the distance between fibres can affect the heating rate. To avoid modelling the matrix and the fibres individually, various studies apply the simplifying assumption that the laminate behaves as a macroscopic homogenous conductive material with equivalent anisotropic properties ([16–20]). This considerably reduces the calculation time of the models.

The in-plane electrical conductivity of a carbon fibre-based laminate is a critical parameter to simulate the induction heating as it controls the temperature distribution in the sample [21]. It can be estimated from the electrical conductivity of the carbon fibre itself, depending on the fibre volume fraction and the ply orientation sequence in the laminate. The rule of mixture (Equation (1)) can be used to calculate the longitudinal electrical conductivity of a ply σ_0 (in the direction of the fibres) [21]:

$$\sigma_0 = \sigma_f \bullet \nu_f + \sigma_m \bullet \left(1 - \nu_f\right) \approx \sigma_f \bullet \nu_f \tag{1}$$

With σ_f and σ_m representing the fibre and matrix electrical conductivity, respectively, and ν_f the fibre volume fraction. As $\sigma_m << \sigma_f$, the second term of the addition can be neglected. The transverse electrical conductivity σ_{90} is also very small compared to the longitudinal one and can be neglected. Then, the electrical conductivity of the laminate is calculated by considering the orientation of each ply. In a $[0,90]_{2S}$ laminate, one half of the plies is in the x-direction and the other half in the y-direction, which means the equivalent electrical conductivity will be equal in both directions. The electrical conductivity in the x-direction can be calculated using Equation (2):

$$\sigma_x = \nu_{fx} \bullet \sigma_0 = f_x \bullet \nu_f \bullet \sigma_0 \tag{2}$$

With f_x representing the fraction of plies in the x-direction. In the case of a $[0,90]_{2S}$ laminate ($f_x = 0.5$) with a fibre volume fraction of 60 %, the electrical conductivity of the laminate equals 0.3 times the fibre electrical conductivity.

Recent work from Van den Berg et al. showed the 6-probe method to be an efficient and reliable way to measure the in-plane anisotropic electrical conductivity of a laminate [22]. Their work also concluded that the rule of mixture based on the carbon fibre conductivity provided a good approximation of the electrical conductivity of the composite laminate, which is why it is retained in this paper.

A wide range of values for the carbon fibre electrical conductivity has been reported in the literature, depending on the fibre type and the measurement method. This variability impacts the equivalent electrical conductivity of the laminate. The electrical conductivities of Tenax HTS45 and other commercially available carbon fibres are summarized in Table 1, also presenting the corresponding laminate electrical conductivities, based on Equation (2). It appears that there is variability in the reported values, but a range between 16000 and 22000 S/m seems to be reasonable.

Table 1
Electrical conductivity values for carbon fibres and laminates from the literature.

Carbon fibre type	Fibre electrical conductivity [S/m]	Equivalent $[0,90]_{2S}$ laminate electrical conductivity ($\nu_f = 60$ %) [S/m]	References
Tenax HTS45	66667	20000	[23]
IM7	67114	20134	[24]
AS4	64935	19481	[24]
AS4	59000	17700	[21]
T1000G	71429	21429	[25]
T700S	62500	18750	[26]
T300	58824	17647	[27]
T300	55556	16667	[28]

The main limitation of this approach is that it does not consider the interactions between non-parallel carbon fibre plies. It has been demonstrated that the number of 0°/90° interfaces in the laminate affects the induction heating. For example, a $[0,90]_{2S}$ and a $[0_2,90_2]_S$ laminate have the same amount of fibres in each direction and the same equivalent electrical conductivity is obtained using the presented rule of mixture (Equation (2)), but they will not heat up the same way, since there are more 0°/90° interfaces in the $[0,90]_{2S}$ assemblies [29]. To correctly predict the heat generation, it is therefore necessary to use a microscale model, which considers each ply separately and calculates their interactions ([20,30–32]). These models are more precise but more complicated to implement and more calculation-intensive than those using the equivalent homogeneous material approximation.

1.3. Sandwich structures

Sandwich structures are used in some applications where a high bending stiffness and low weight are required. They are composed of two skins – or facesheets – at the top and bottom of a low-density core, which can be a cellular structure (honeycomb, corrugated, etc.) or a foam [33]. The skins are typically made of carbon fibre reinforced thermoset composites or aluminium. The cores can be made of a large variety of materials and geometries, from Nomex and aluminium honeycombs to polymeric foams. The skin-core assembly, which is required to transfer the loads across the structure, is usually accomplished through adhesive bonding. Recently, the interest for all-thermoplastic sandwich panels has been growing, as these materials present the advantages of being potentially repairable and recycled ([34,35]). However, the use of thermoplastic polymers requires adapting the skin-core joining method, as adhesive bonding usually requires extensive surface preparation and can lead to low mechanical properties [36].

The use of welding for this joining step is evaluated as an alternative. It is reported that the assembly of sandwich structures by thermoplastic welding can by done in two ways: isothermally, where the pressure is applied during heating of the parts, and non-isothermally, where the parts are first heated, then transferred to a secondary device in which pressure is applied to consolidate the parts together [37]. The pressure is applied by placing parts in a vacuum bag ([38–40]), by compression moulding in a hot press ([41–43]) or by double-belt lamination ([44,45]). In these methods, either the whole part is heated up, making the core prone to collapse under the applied pressure and causing the facesheets to deconsolidate, or heat is lost during parts transfer when laminates skins are heated up separately, requiring them to be overheated.

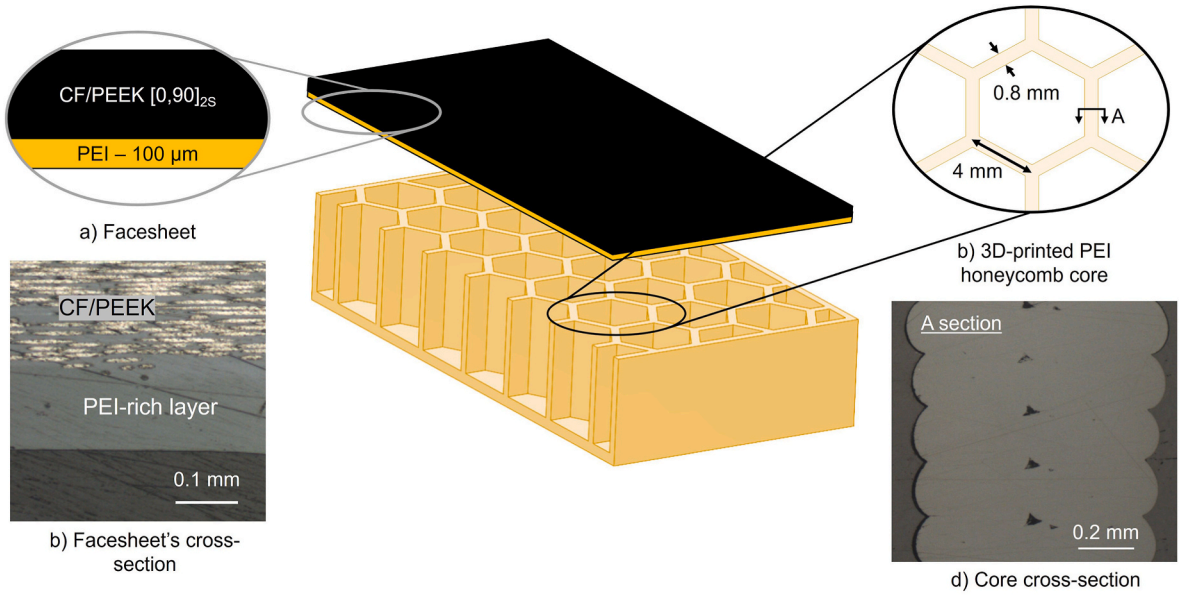

Fig. 2. Scheme of a sandwich sample, with close-up view on (a) the composite facesheet made of CF/PEEK laminate with a co-consolidated PEI layer, (b) an optical microscopy cross-section image of the facesheet, with the co-consolidated PEI layer highlighted by the white line, (c) the 3D-printed PEI honeycomb core with the cells dimensions, and (d) an optical microscopy cross-section image of the printed core.

In a previous work from the authors, glass fibre thermoplastic composite facesheets were joined to a thermoplastic polymer core by induction welding, using a hysteresis-losses susceptor placed at the interface between the skins and the core [46]. In that case, heat was generated directly at the joining interface instead of across the complete structure. This method demonstrated the advantages of welding as a joining technique to manufacture sandwich panels. The use of a susceptor was necessary to join glass fibre facesheets. In the case of carbon fibre facesheets, a susceptor located at the weld interface may not be necessary because it would be possible to heat up the carbon fibre directly. In such a case, the facesheets would likely be heated across their entire thickness, as opposed to a local heating at the joint interface when a susceptor is used.

The goal of the present study is to join skins made of carbon fibre reinforced poly-ether-ether-ketone (CF/PEEK) laminate to a honeycomb core made of poly-ether-imide (PEI). The induction heating behaviour of the laminate must first be analyzed to determine the induction welding parameters that can be used to weld the facesheets to the core, in order to produce sandwich panels. As edge effects, and therefore overheating that could lead to core crushing, are expected at the edges of the panels, it is proposed to increase the sandwich skin dimensions compared to the core of the sandwich structure to be welded. This will reduce edge effects – or localise them in the sacrificial skin length – and allow for a more homogeneous temperature distribution along the weld line with the core. As previously demonstrated, the use of the Thermabond process on the sandwich skins can be applied to sandwich structures [47]. This method consists in co-consolidating a layer of PEI at the surface of the CF/PEEK laminate ([48,49]), which is possible due to the miscibility of PEEK and PEI [50]. This allows welding to occur at temperatures in the range of 280–300 °C, i.e., lower than the melting point of PEEK (343 °C). Remaining below the PEEK melting temperature reduces the risk of core crushing and skin deconsolidation while ensuring skin-core PEI-PEI joining by thermoplastic welding [47].

The induction heating of CF/PEEK skins of various dimensions is first characterized experimentally and compared to a finite element model, to verify its accuracy and its capability to predict heat generation and the temperature distribution in the laminates. Then, 3D-printed PEI honeycomb cores are assembled to the CF/PEEK thermoplastic composite skins comprising a layer of PEI at their surface using the vacuum induction welding (Vac-IW) technique [46] without a susceptor, i.e., by direct heating of the skins' carbon fibre. Finally, the quality of the weld is assessed by testing the sandwich panels under the flatwise mechanical tensile test and the failure modes are reported.

2. Methodology

2.1. Samples manufacturing

PEEK is selected as the composite matrix due to its high mechanical properties and high service temperature, and because it was used in previous studies reported in the literature, alongside other poly-aryl-ether-ketone polymers such as poly-ether-ketone-ketone (PEKK). PEI is retained due to its compatibility and miscibility with PEEK [50], and because it exhibits a processing temperature inferior to the melting point of PEEK.

Composite laminates are manufactured using CF/PEEK unidirectional prepreg (Tenax®-E TPUD PEEK-HTS45 from Teijin) in a $[0,90]_{2S}$ lay-up sequence [51]. The consolidation is done by compression moulding in a hot press for 20 min at 380 °C and 2 MPa. The resulting 8-ply laminates exhibit a thickness of 1.1 mm. They are cut into 5 cm-long samples of various widths. These samples are to be heated by induction to obtain their surface temperature distribution as a function of time.

Similar samples are produced to be induction-welded to thermoplastic polymeric cores. They are made of the same CF/PEEK lay-up with an additional 100 µm-thick layer of PEI at the surface, based on the Thermabond process ([48,49]). Thus, the resulting laminate presents a co-consolidated surface layer of PEI in the area that is welded to the PEI core. The PEI layer is added at the surface of the laminate during the consolidation process. The addition of the PEI film is done during the manufacturing of the laminate, without an impact on the manufacturing time or cost.

The honeycomb cores are manufactured by 3D-printing using an AON3D M2 printer equipped with a 0.4 mm nozzle. The samples have a surface of 5 cm by 5 cm and a height of 11 mm, including a 1 mm thick bottom skin, also 3D-printed from PEI. Hexagonal honeycomb cells have a side length of 4 mm. The cell wall thickness is 0.8 mm. The material used for 3D-printing is an ULTEM 1010 filament with a 1.75 mm

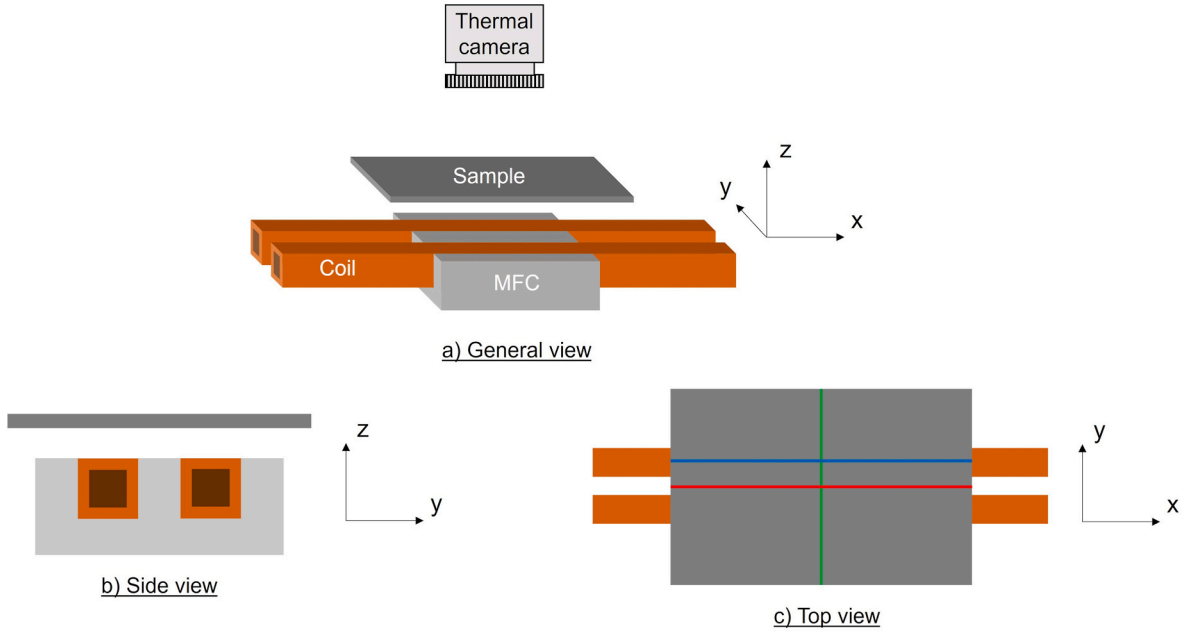

Fig. 3. Scheme of the static induction heating setup. (a) General view of the setup, with the thermal camera located above the sample to record temperature evolution. (b) Side view showing the induction coil profile. The distance between the sample and the coil is defined as the coupling distance. (c) Top view of the setup as seen by the thermal camera, with the three lines of interest highlighted in green (center profile), red and blue (center and 5 mm width profiles). (For interpretation of the references to colour in this figure legend, the reader is referred to the Web version of this article.)

diameter (3DxTech). The nozzle temperature is fixed at 390 °C, the printing bed at 160 °C and the printing chamber at 135 °C. The layer height is 0.2 mm, and the printing speed 30 mm/s. Nano-polymer adhesive (Vision Miner) is applied onto the printing bed to improve part's adhesion and minimize warping. The complete sandwich structure to be welded is summarized in Fig. 2.

2.2. Static induction heating

To characterize the induction heating of CF/PEEK skins, a tailored setup (Fig. 3a/b) including a hairpin copper coil equipped with a magnetic field concentrator (MFC) is used [52]. The sample is placed on a Kapton film that keeps it suspended above the coil at coupling distance of 4 mm. A FLIR A700 thermal camera records the thermal evolution of the static sample during a heating period of 90 s. The alternating current amplitude is varied in the range of 50 A–100 A, and the frequency is automatically adjusted by the generator to match the resonance frequency of the system. This frequency depends on the current, the size of the MFC, the coil geometry and the interaction with the sample.

The emissivity of the laminate is determined by heating up a sample on a heating plate, and by recording the temperature at the surface simultaneously with a thermocouple and the thermal camera, initially with an emissivity set at 1. The emissivity is then reduced until the reading of the thermocouple and the thermal camera are matching, which happens with an emissivity of 0.95 in this case. This corresponds to what was reported in the literature [10].

The temperature distribution on the surface facing the thermal camera (opposite to the induction coil) is first extracted from thermal camera imaging. Then, the temperature distribution is measured along three lines of interest on the sample, as presented in Fig. 3c: the center profile temperature (in green), the center width profile (in red) and the 5 mm width profile (in blue), which is parallel to the central width but 5 mm away from the center of the induction coil.

2.3. Induction heating finite element model

A 3D finite element model of the induction heating process is developed using the COMSOL Multiphysics 6.1 software. The model simulates the electromagnetic field around the coil and the heat generation in the carbon fibre composite laminate located above the coil. The magnetic field amplitude is calculated first in the frequency domain and kept constant during the duration of the simulation. This reduces the calculation time compared to recalculating the magnetic field at each time step. Then, heat transfer is modelled in a subsequent time-dependant step. Coupling between the two physics is done by considering the electromagnetic losses due to the induced eddy currents in the magnetic step as the heat source of the heat transfer step. Heat conduction inside the laminate is considered, and radiation and convection boundary conditions are imposed on the laminate's surface, allowing to calculate the temperature evolution inside the laminate over time. The geometry of the model, reproducing the induction heating setup schematized in Fig. 3a–is presented in Fig. 4. A mesh composed of free

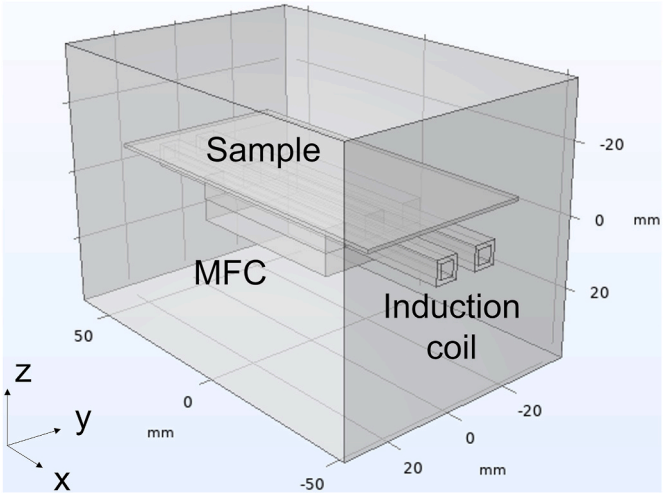

Figs. 4. 3D geometry of the static induction heating setup model in COMSOL Multiphysics.

Table 2
Materials properties used in the COMSOL Multiphysics induction heating simulations.

	CF/PEEK $[0,90]_{2S}$	Copper coil	Magnetic field concentrator	Air
Density [kg/m^3]	1600 (at 25 °C) [54] Density as f(T) is used in the model	–	–	–
Specific heat capacity [J/kg·K]	860 (at 25 °C) [54] Specific heat capacity as f(T) is used in the model	–	–	–
Thermal conductivity [W/m·K]	3.5 (in-plane) [53] 0.335 (out-of-plane) [53]	–	–	–
Electrical conductivity [S/m]	Defined based on experimental results	6e7 [17]	6.66e-3 [16]	1 [15]
Magnetic relative permeability [−]	1 [21]	1 [17]	16 [16]	1 [17]
Electrical relative permittivity [−]	3.7 [21]	1 [17]	1 [16]	1 [17]

tetrahedral elements is automatically generated by COMSOL Multiphysics. The PARADISO implicit direct solver is used for the simulation, and the maximum calculation time step is set at 2 s.

The different materials properties used in the model are reported in Table 2. The thermal conductivity of the CF/PEEK laminate is considered as temperature-independent [53]. Temperature-dependent density and specific heat capacity are modelled as reported in the literature [54]. As presented in the introduction, the homogenized in-plane electrical conductivity of the laminate is an important property to obtain reliable induction heating simulations. As the electrical conductivity of the TENAX-E HTS45 carbon fibre used in this work has not been characterized, a first induction heating measurement is employed to define the equivalent electrical conductivity of the laminate and "calibrate" the model for the tested laminate configuration. The obtained value then remains unchanged for the remaining simulations. As the $[0,90]_{2S}$ laminate is symmetric and balanced, with half the fibres in the 0° and the other half in the 90° directions, the equivalent electrical conductivity of the laminate is the same for both fibre directions in the plane. The convection coefficient is fixed at 5 W/m·K [54] and the emissivity at 0.95 [10].

The potential heating of the coil and the MFC, which might affect the magnetic field generation and the laminate heating are neglected. Indeed, these contributions are minimal in the current amplitude range used in the experiments as the coil is water-cooled, which also cools down the MFC. Consequently, the temperature evolution is only calculated in the laminate samples, and not in the coil, the MFC or the surrounding air.

2.4. Continuous induction welding setup

To weld CF/PEEK skins to 3D-printed honeycomb cores, pressure must be applied on the sample during heating and cooling to ensure the complete development of the welding degree. In this study, vacuum induction welding (Vac-IW) is used [46]. To ensure the continuous application of pressure throughout the process, the sample is placed inside a vacuum bag. Then, the induction coil moves linearly relative to the sample at a constant speed and progressively heats up the skin and the core located close to the interface. The sample is kept under pressure after the passage of the coil for 10 min to ensure the temperature is getting below the glass transition temperature of PEI. The applied atmospheric pressure (0.1 MPa), which would be insufficient for properly welding or consolidating high performance thermoplastic composites, is here taken by the walls of the core cells. The pressure taken by the core cell walls corresponds to an approximate value of 0.5 MPa, which is in the range of adequate welding pressures for thermoplastic composites. This value is obtained by assuming that the core cell walls, which are covering around 20 % of the core surface area, are supporting the totality of the applied pressure, increasing the effective pressure on the weld line to 0.5 MPa.

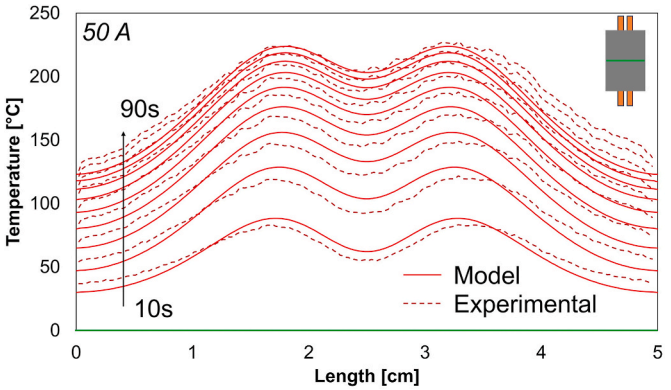

Fig. 5. Induction heating of a 10 cm by 5 cm laminate under a 50 A current amplitude. The measured temperature along the center profile of the sample is reported every 10 s for 90 s and compared to the model's results.

2.5. Sandwich structures characterization

Two types of characterization are conducted on the welded sandwich structures. First, the skin/core welding interface is observed by optical microscopy (Olympus GX51) to verify that a complete contact between the skin and the core was reached, and to analyze the amount of deformation at the top of the cell walls. Then, skin-core strength is measured by performing flatwise tensile (FWT) tests, following the ASTM C297 standard. A Hysol EA9696 epoxy film is used to bond the steel blocks to the sandwich samples to perform the FWT measurement. Finally, visual fracture analysis is used to assess the type of failure at the joining interface and the quality and homogeneity of the weld. If the visual analysis of a fractured sample reveals that a printing defect was present and caused an early core failure, the sample is discarded and not considered in the FWT results.

3. Results

3.1. Experiment-derived electrical conductivity

The first induction heating measurement is performed on a 5 cm by 10 cm laminate sample induction-heated with a current amplitude of 50 A. The temperature along the center profile line is extracted from the thermal camera measurements every 10 s for 90 s. Considering a conductivity of 22000 S/m allows to obtain the closest correspondence between the experimental and the simulation curves, as shown in Fig. 5. This is in agreement with the expected electrical conductivity of the Tenax HTS45 fibre reported in Table 1. The general shape of the curve in the model matches with the experimental results, and the evolution with time also corresponds very well. Therefore, the electrical conductivity of the CF/PEEK laminates is fixed at 22000 S/m for all the other simulations.

This value for the equivalent homogeneous electrical conductivity of the laminate is 10 % higher than the one presented in Table 1 for the same fibre. As discussed, the difference between the two values might be caused by the fact that the rule of mixture does not consider any heating mechanism at the point of contact between non-parallel fibres. This region also generates heat through contact resistance or dielectric heating, which probably explains why a larger apparent electrical conductivity is observed. The 10 % error can be attributed to uncertainties

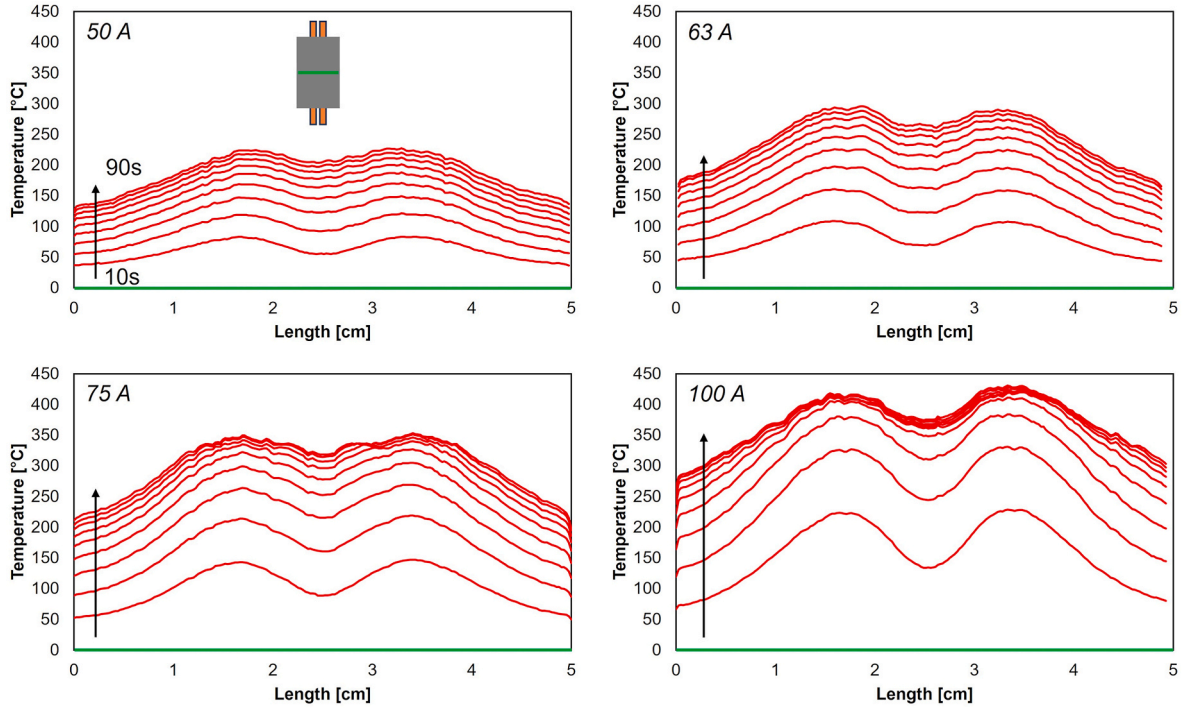

Fig. 6. Induction heating of 10 cm by 5 cm laminates under varying current amplitudes. The measured temperature along the center profile of the sample is reported every 10 s for 90 s.

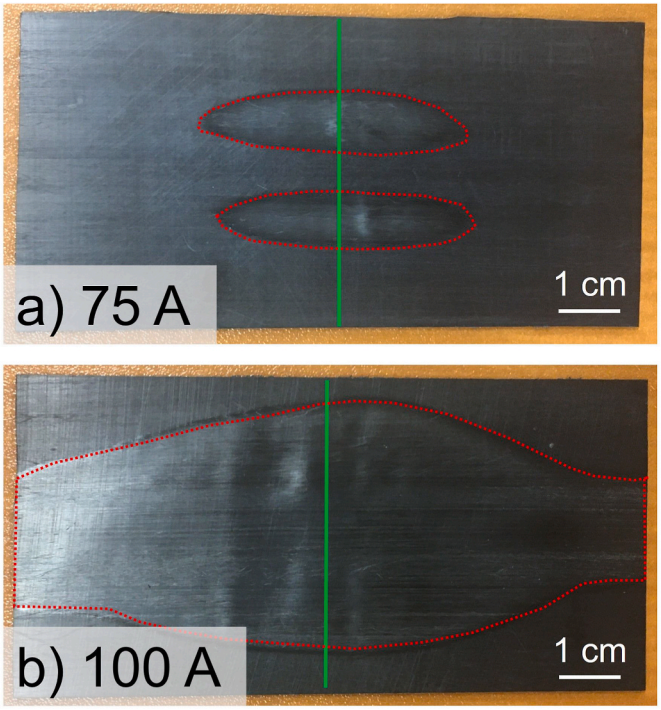

Fig. 7. Pictures of samples heated by induction under a current of (a) 75 A and (b) 100 A after 90 s. The green line highlights the location of the temperature profile reported in Fig. 6. The areas where the CF/PEEK laminate deconsolidated are shown with the red dotted lines. (For interpretation of the references to colour in this figure legend, the reader is referred to the Web version of this article.)

in the thermal model (magnetic field amplitude, convection coefficient, emissivity) or to the experimental measurements conducted with the thermal camera.

The model diverges slightly from the experimental results on the edges as time and temperature increase. The model boundary conditions at the edges or the meshing in that area might be responsible for the difference. This should be addressed to obtain a more reliable model, but is satisfactory for purposes of the present study, as the general shape and evolution of the temperature profile is correctly predicted.

3.2. Current amplitude influence on induction heating

The experimental temperatures reached during induction heating under current values of 50 A, 63 A, 75 A and 100 A are presented in Fig. 6 as a function of the location along the length of the CF/PEEK laminates. These current amplitudes were selected after preliminary tests showed that the melting point of the PEEK matrix was not reached at 50A, but that a large surface of the laminate was molten and deconsolidated at 100A. Intermediate measurements conducted at 63A and 75A are then added to verify the evolution of the temperature profile

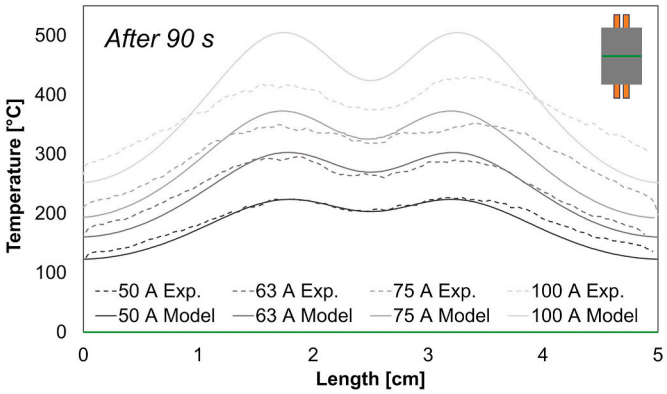

Fig. 8. Induction heating of 10 cm × 5 cm laminates under varying current amplitudes. The temperature distribution along the center profile line is reported. Only the temperature after 90 s is shown for clarity. Experimental measurements (dashed lines) are compared to simulations (solid lines).

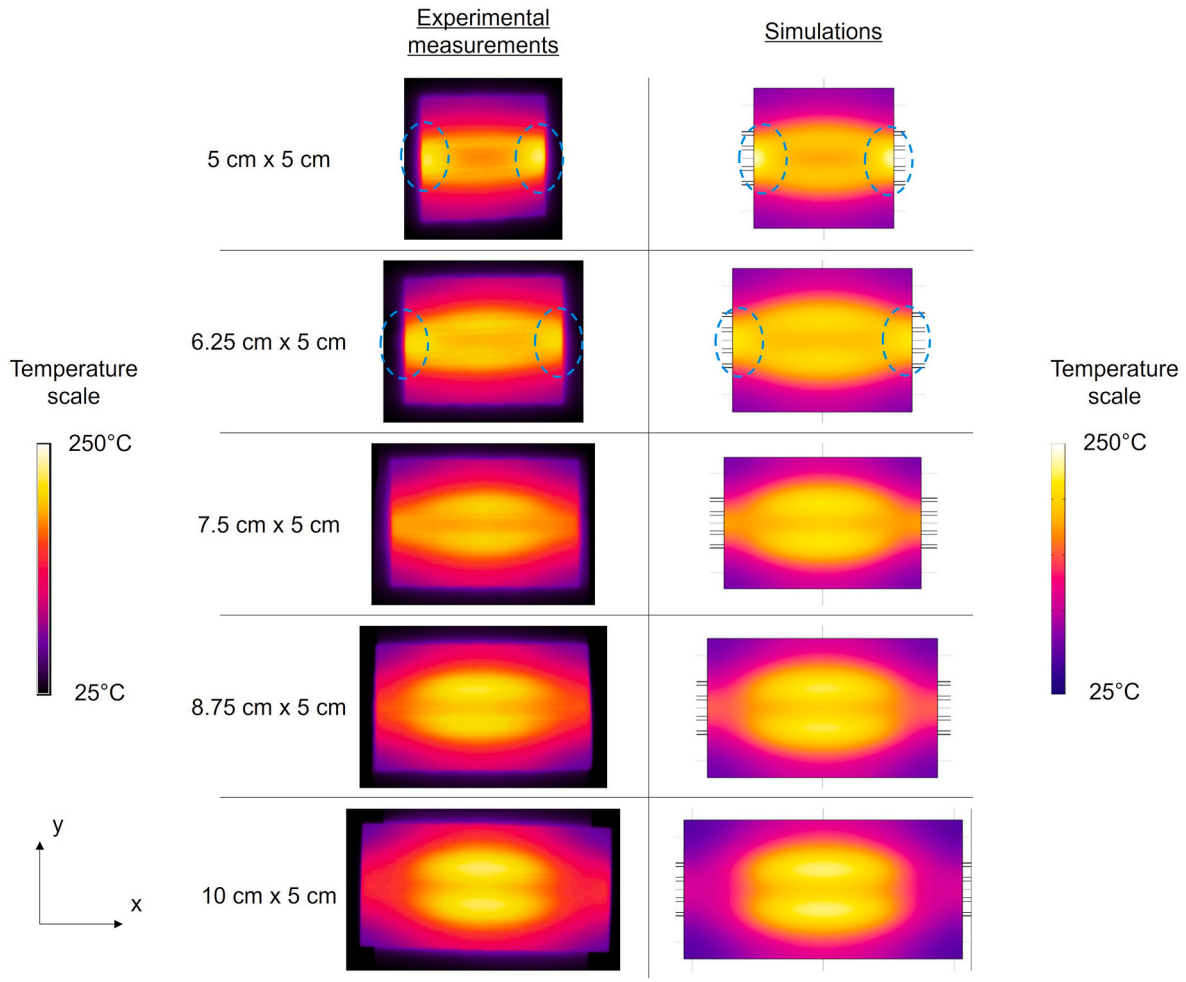

Fig. 9. Temperature distribution on the CF/PEEK samples surface under a 50 A current for varying samples widths. Experimental results as recorded by the thermal camera are compared to simulations. Edge effects are highlighted by the blue circles. The induction coil is located behind the samples and is orientated vertically. (For interpretation of the references to colour in this figure legend, the reader is referred to the Web version of this article.)

under varying field amplitudes and validate that the model can follow this change. The temperatures along the center profile line are extracted every 10 s during the 90 s of heating. As expected, it appears that a higher current amplitude leads to a higher temperature induced by eddy currents. The maximum recorded temperature after 90 s of heating is 225 °C at 50 A, 298 °C at 63 A, 362 °C at 75 A and 435 °C at 100 A. Both the samples heated at 75 A and 100 A reached the melting point of PEEK (343 °C). Signs of deconsolidation are visible on these two samples after the heating test, as presented in Fig. 7. As explained, it is preferable to avoid reaching the melting point of PEEK to prevent laminate deconsolidation. Thus, a current amplitude of 100 A is too high in that configuration and should be avoided. On the other hand, the welding temperature of PEI (around 270–280 °C minimum) was not reached under a current of 50 A. Therefore, an electrical current in the range of 63 A–75 A should be acceptable to perform induction welding with these CF/PEEK laminates.

The experimental temperature curves are then compared with those predicted by the finite element model. Fig. 8 shows a comparison between the simulation and the experiments after 90 s of heating under the various electrical current amplitudes. The model captures well the heating behaviour of the laminates, with some previously noted deviations close to the edges. The 75 A sample presents an asymmetrical curve, showing there might be some defects like fibre misalignment in the right side of the part. The left side of the curve on the other hand fits well with the model. Considerable disagreement is seen in Fig. 8 between the model and the experiment when the laminate reaches high temperatures (e.g. 100 A curve). As shown above, the high 100 A current amplitude led to deconsolidation of the CF/PEEK laminates after 90 s, as shown in Fig. 7. Once deconsolidation occurs, the heat generation and heat transfer are affected because the carbon fibre plies are no longer in physical contact, which reduces the eddy current generation in the laminate as well as the heat conduction in the thickness of the laminate. In that situation, the model is no longer representative of the heating mechanisms and heat transfer in the laminate.

3.3. Impact of the sample width on the temperature profile

The second part of the induction heating characterization consists in observing the temperature profile along the width of the CF/PEEK laminate, for varying sample widths. Varying the width of the samples is expected to impact the edge effects. Measurements are conducted at 50 A to avoid deconsolidating the samples, thus allowing reuse.

First, the complete temperature field recorded by the thermal camera after 90 s is presented in Fig. 9. One can notice the presence of important edge effects in the 5 cm-wide and the 6.25 cm-wide sample (areas of high temperature located close to the edges, as highlighted by the blue circles in Fig. 9). Some edge effects are also visible for the 7.5 cm-wide sample, while larger samples did not produce any visible edge effects. The reduction and elimination of edge effects is caused by the fact that the MFC remains 5 cm-wide, which means that wider samples do not have their edges close to it anymore, but rather in areas where the magnetic field amplitude is lower. The model correctly predicts the

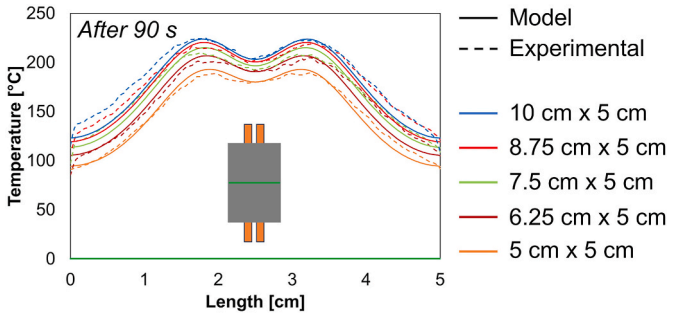

Fig. 10. Induction heating of laminates under 50 A current amplitude for varying sample widths. The temperature distribution along the center profile is reported. Only the temperature after 90 s is shown for clarity. Experimental measurements (dashed lines) are compared to simulations (solid lines).

temperature distribution in the laminate samples during induction heating. It can adapt to the change of width and anticipate the elimination of the edge effects for larger samples with the heat concentrated in the center of the laminates.

Then, the center line profile temperature distribution (Fig. 3c green line) is analyzed. As observed in the dashed line of Fig. 10, it appears that the maximum temperature reached on the samples decreases as the width decreases, from 224 °C for a 10 cm wide sample down to 188 °C for a 5 cm wide sample. This decrease in temperature indicates that a slower welding speed or a higher current amplitude will be required to weld those narrow skins. The curves are then compared to the simulated temperature distributions (solid lines in Fig. 10). The blue curve was used in Fig. 5 to calibrate the model. It appears that the model can correctly predict the variation of temperature observed experimentally, which would help predict the impact of changing the laminate dimensions.

Finally, temperature is extracted for both width profile lines of interest (red and blue in Fig. 3c) and the results are presented in Fig. 11. The x-axis is fixed at zero for the left edge of the 5 cm-wide sample, and the wider samples are centered compared to it. This gives more clarity to compare the samples among themselves. The length that would be welded to the honeycomb core is then located between 0 and 5 mm on the x-axis. It appears that there is a significant change of curvature. As it was observed on the temperature distributions (Fig. 9), edge effects are reduced when the width of the sample increases. The objective is to have a more homogeneous temperature distribution along the width of the sample during the induction welding process.

These results confirm that the 5 cm-wide skin seems unfavorable for sandwich structures of similar width, as it would be impossible to prevent the edge effects and the related non-homogeneous degree of welding along the width. The same observation can be made for large skins (8.75 and 10 cm-wide), which lead to more heat generation in the center of the laminate, inducing a lower degree of welding close to the edges. Therefore, out of the presented curves, it seems that 6.25 cm and 7.5 cm-wide samples exhibit the most favorable heating behaviour with the most homogeneous temperature distribution along the width.

The temperature distribution along the lines of interests of the samples is also calculated with the model to verify its accuracy. The curves are compared with the presented experimental results. For the center profile as shown in Fig. 10, the model can correctly predict the reduction of the temperature at shorter widths. The shape of the temperature profile is also correctly predicted, which further confirms the quality of the model. For the width profile, the model diverges from the experimental results when getting farther away from the center.

3.4. Optical microscopy on welded sandwich structures

The welding lines of the induction welded sandwich samples are first observed by optical microscopy, with a focus on the evolution of the cell wall deformation at the point of contact with the skin. This is the point where heat is generated and where welding occurs. Fig. 12 presents the

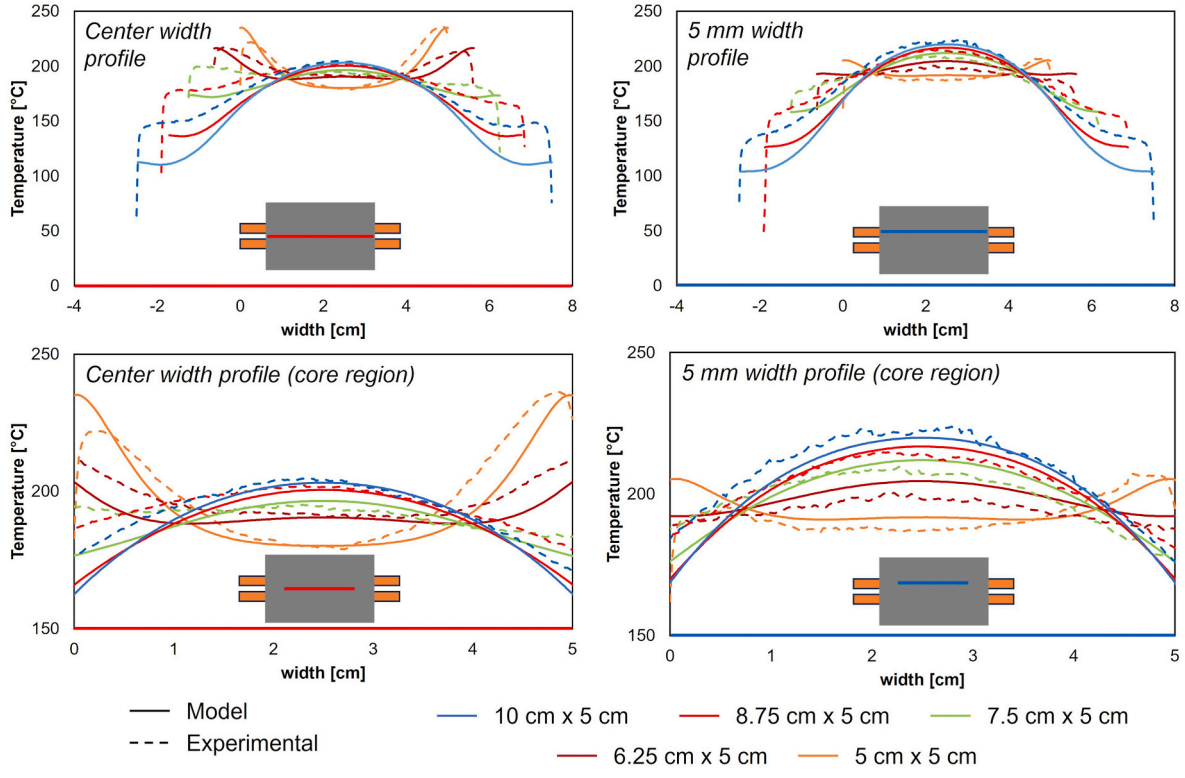

Fig. 11. Induction heating of laminates under 50 A current amplitude for varying sample widths. The temperature distribution along both width profiles is reported. Only the temperature after 90 s is shown for clarity. Experimental measurements (dashed lines) are compared to simulations (solid lines).

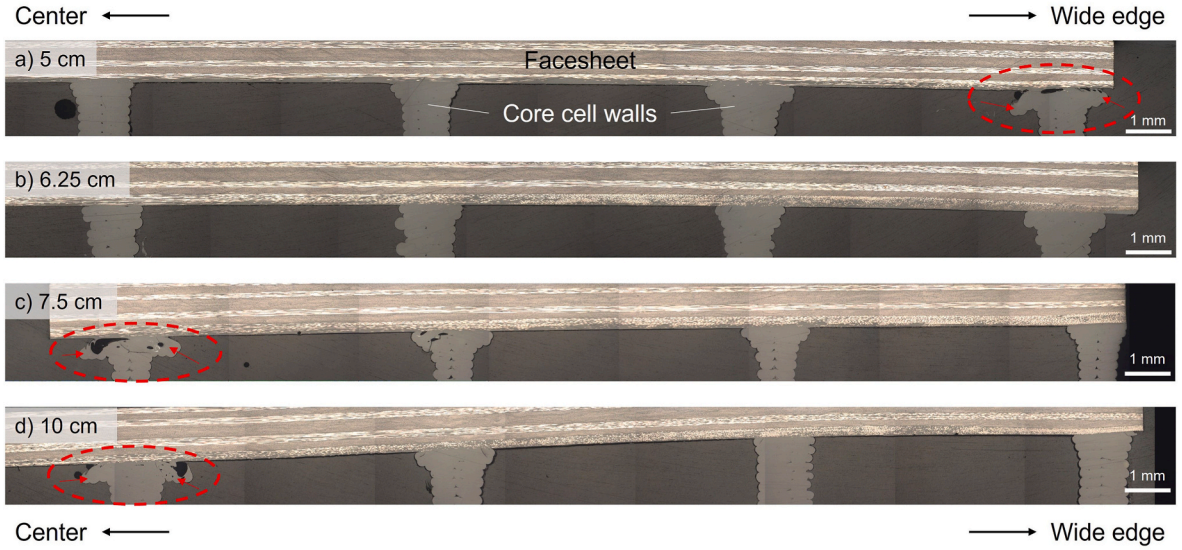

Fig. 12. Optical microscopy images for sandwich samples welded by induction. The welding profile is shown for samples with varying skin widths: (a) 5 cm, (b) 6.25 cm, (c) 7.5 cm and (d) 10 cm. The left side of the figure corresponds to the center of the welded sample's cross-section, while the right side corresponds to its wide edge. The cell walls that experienced overheating and crushing are shown by the dashed red circles. The deformed wall are highlighted by the red arrows. (For interpretation of the references to colour in this figure legend, the reader is referred to the Web version of this article.)

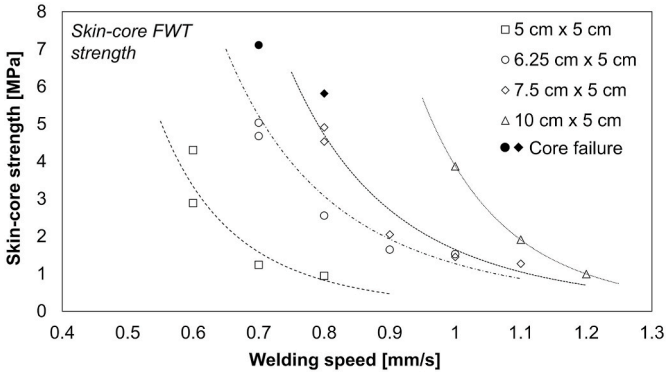

Fig. 13. Skin-core FWT strength of induction welded sandwich structures as a function of the welding speed. Each point represents one measurement. Dashed/dotted trend lines are guides to identify more clearly each dataset. Core failure is indicated by filled black data points.

optical micrographs of the sandwich cross section for samples welded with skins width of 5, 6.25, 7.5 and 10 cm skins. 8.75 cm-wide samples are not further evaluated as their heating profile is very similar to the 10 cm-wide ones.

With a 5 cm-wide skin, presented in Fig. 12a, more heat was generated close to the edge as this is where the cell wall is the most deformed. This agrees with the temperature distribution observed by thermal imaging, resulting from edge effects. As expected, this sample exhibits a non-homogeneous welding profile that will lead to non-homogeneous weld. On the other hand, the opposite behaviour is observed in Fig. 12c, welded with a 7.5 cm-wide skin and Fig. 12d, with a 10 cm-wide skin. The use of a wider skin leads to more heat generation in the center of the sample and therefore more visible deformation in that area. It even appears on the optical microscopy images that the laminate started to deform in the center, highlighting the large heating induced in that region. Overall, the non-homogeneity of the heat generation appears clearly in the samples with extreme skin widths. It is expected that these samples will consequently exhibit a non-homogeneous degree of welding along their width. The sample welded

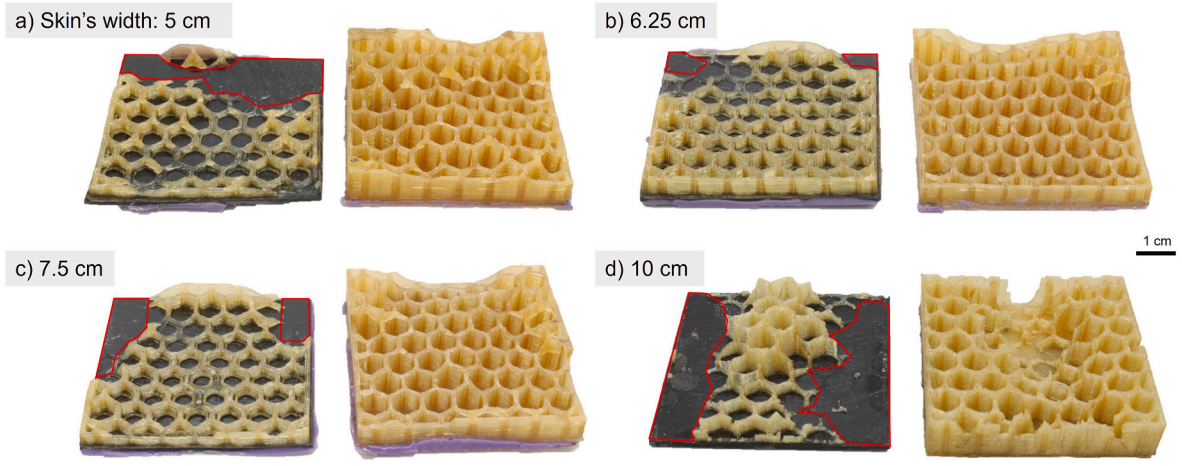

Fig. 14. Fractured induction welded sandwich samples. The samples were welded using a skin's width of (a) 5 cm, (b) 6.25 cm, (c) 7.5 cm, (d) 10 cm. The red lines correspond to the surface areas where adhesive failure occurred. (For interpretation of the references to colour in this figure legend, the reader is referred to the Web version of this article.)

with a 6.25 cm-wide skin (Fig. 12b) exhibits the most homogeneous heating, as the deformation of the cell walls is similar on the four walls along the width. This also agrees with the thermal imaging results, which show that the temperature profile with that skin width was the most uniform.

Decreasing the welding speed will allow previously less heated areas to be heated up enough, letting them reach higher degree of welding. But at the same time, the other areas of the sample will certainly overheat, leading to core crushing, as it started to be observed in Fig. 12c and d, and skin deconsolidation. Non-homogeneity of the temperature distribution cannot be compensated by adjusting the speed, which highlights the interest of correctly choosing the skin's width to provide a homogeneous temperature profile. Optical microscopy results also confirm that choosing 6.25 cm-wide skins is appropriate.

3.5. Skin-core strength

The skin-core strength of welded sandwich specimens is characterized by performing FWT mechanical tests. The resulting skin-core strengths of the welded samples are reported in Fig. 13. Each data point on the graph represents one FWT test. Three samples were tested for the higher strength samples (at 0.7 mm/s for the 6.25 cm-wide skins and at 0.8 mm/s for the 7.5 cm-wide skins) to validate the repeatability of the method. The optimal welding speed is defined as the speed at which the highest skin-core strength is reached without observing core crushing on the sample. Fractured sandwich samples are then visually analyzed to observe the failure mode and the homogeneity of the degree of welding. One representative sample for each skin's width welded at optimal speed are presented in Fig. 14.

It can first be observed in Fig. 13 that, for a given skin's width, reducing the welding speed increases the maximum skin-core strength. This trend was expected as the laminate spends more time under the induction coil at lower speed, therefore reaching higher temperatures and maintaining them for a longer duration [19]. Secondly, a larger optimal welding speed is obtained with the use of wider skins. This corresponds to the observation made in Fig. 10 where it was seen that a wider skin leads to a higher temperature in the laminate.

However, the use of 10 cm wide skins also leads to non-homogeneous heating, as observed in optical microscopy images (Fig. 12). It is also confirmed by observing the fractured samples (Fig. 14d), where it appears that the failure mode is adhesive close to the edges with a transition to a core failure in the center, highlighting the higher degree of welding in that area. The fraction of the surface over which adhesive failure occurred (shown by the red lines in Fig. 14a) is evaluated at 43.5 %. When the skin's width is reduced to 7.5 and 6.25 cm, the optimal welding speed becomes smaller, but the maximum strength increases, as a homogeneous heating and homogeneous degree of welding are reached at the skin/core interface. When observing fractured sandwich samples (Fig. 14b and c), it also appears that the failure mode is mostly core failure (95.6 % and 89.6 % of the surface in Fig. 14b and c, respectively), which tends to indicate that the dominant characteristic for the flatwise tensile strength is the strength of the 3D-printed core itself. The weld surpasses the resistance of the core, indicating its high quality. The experimental skin/core strength then decreases again for 5 cm-wide skins, which once again is probably caused by a non-homogeneous heating along the skin's width, although it is less visible in Fig. 14a. The adhesive failure is reported on 18.9 % of the surface on that sample. Based on the results, the 7.5 cm-wide skins welded at 0.8 mm/s and the 6.25 cm-wide skins welded at 0.7 mm/s present the best mechanical properties. The optimal choice would depend on the desired balance between the welding speed and the amount of excess skin to be trimmed after welding.

Overall, the maximum measured skin-core strengths range between 5 and 7 MPa for the six tested sandwich samples that were welded using 6.25 and 7.5 cm-wide skins. This is higher than what is reported in different articles characterizing sandwich structures with flat-wise tensile tests. Widagdo et al. (CF/epoxy skins bonded to glass fibres/phenolic resin honeycomb core with FM-300 adhesive) and Hegde et al. (CF/cyanate ester skins bonded to Kevlar/phenolic resin honeycomb core with epoxy film adhesive) reported maximum strength between 5 and 5.2 MPa ([55,56]). Butukuri et al. (CF/epoxy skins to honeycomb core with FM-300 adhesive) reported similar strengths for Nomex cores, and higher strengths only for aluminium cores [57]. For polymer-based sandwich structures, the presented vacuum induction welding method shows higher results than other structures assembled by adhesive bonding, with the advantages of minimal surface preparation and a shorter processing time.

4. Conclusion

This paper presents a susceptor-less method to join CF/PEEK skins to honeycomb cores produced by 3D-printing. The heat generated inside the skin due to induced eddy currents allows for the weld to happen. To handle the edge effects that are typically observed in conductive materials during induction welding, it is proposed to add sacrificial length to the CF/PEEK skin in which edge effects can occur, leaving the effective surface area of the skin in contact with the core to experience homogeneous heating.

The heating behaviour of the laminate is observed by thermal imaging, validating the benefit of using extra width on the skin to limit edge effects. A 3D model on COMSOL Multiphysics is then presented to predict the temperature profile of the samples during the process, at variable sample widths and induction current values. The good agreement between the simulations and the experimental results shows that the COMSOL model can be used as a tool to predict the impact of changing the current or increasing the sample dimensions. This can help engineers minimize the number of trials necessary to characterize induction welding and better predict the welding by induction.

Finally, induction welding of sandwich samples is performed to validate the assembly of sandwich panels by induction welding. The application of the Thermabond process allows to weld by induction at a lower temperature, avoiding deconsolidation in the facesheets and reducing the risk of core crushing. Flatwise tensile tests show that higher skin-core strength can be reached with this process, compared to other reported methods. Fracture analysis of tested samples confirms the non-homogeneous heating when using too wide or too narrow skins, and its consequences on the weld quality. This shows the benefits of selecting an optimal set of dimensions for the facesheet laminate.

CRediT authorship contribution statement

Romain G. Martin: Writing – original draft, Software, Methodology, Investigation, Data curation, Conceptualization. **Christer Johansson:** Writing – review & editing, Supervision. **Jason R. Tavares:** Writing – review & editing, Supervision. **Martine Dubé:** Writing – review & editing, Supervision.

Declaration of competing interest

The authors declare that they have no known competing financial interests or personal relationships that could have appeared to influence the work reported in this paper.

Data availability

Data will be made available on request.

Acknowledgements

This work was funded by CREPEC (Research Center for High Performance Polymer and Composite Systems), NSERC (Natural Sciences and Engineering Research Council of Canada) (grant number ALLRP

556497-20), PRIMA Québec (Pôle de Recherche et d'Innovation en Matériaux Avancés) (grant number R20-13-004), the Canadian Space Agency (CSA), Ariane Group, NanoXplore inc, Mëkanic and Dyze Design.

References

[1] Ageorges C, Ye L, Hou M. Advances in fusion bonding techniques for joining thermoplastic matrix composites: a review. Compos Part A Appl Sci Manuf Jun. 2001;32:839–57.
[2] Yousefpour A, Hojjati M, Immarigeon JP. Fusion bonding/welding of thermoplastic composites. J Thermoplast Compos Mater Jul. 2004;17(4):303–41.
[3] Van Ingen JW, Buitenhuis A, Wijngaarden M, Simmons F. Development of the Gulfstream G650 induction welded thermoplastic elevators and rudder. May 2010.
[4] Ahmed TJ, Stavrov D, Bersee HEN, Beukers A. Induction welding of thermoplastic composites—an overview. Compos Part A Appl Sci Manuf Oct. 2006;37(10):1638–51.
[5] Bayerl T, Duhovic M, Mitschang P, Bhattacharyya D. The heating of polymer composites by electromagnetic induction – a review. Compos Part A Appl Sci Manuf Feb. 2014;57:27–40.
[6] Suwanwatana W, Yarlagadda S, Gillespie JW. Hysteresis heating-based induction bonding of thermoplastic composites. Compos Sci Technol Sep. 2006;66(11):1713–23.
[7] Martin RG, Johansson C, Tavares JR, Dubé M. Material selection methodology for an induction welding magnetic susceptor based on hysteresis losses. Adv Eng Mater 2022;24(3).
[8] Wetzel ED and Fink BK. Feasibility of magnetic particle films for curie temperature-controlled processing of composite materials. p. 83.
[9] Rudolf R, Mitschang P, Neitzel M. Induction heating of continuous carbon-fibre-reinforced thermoplastics. Compos Part A Appl Sci Manuf Nov. 2000;31:1191–202.
[10] Mitschang P, Rudolf R, Neitzel M. Continuous induction welding process, modelling and realisation. J Thermoplast Compos Mater Mar. 2002;15:127–53.
[11] Kane B, Wasselynck G, Bui HK, Trichet D, Berthiau G. Focalization of electromagnetic power at the interface between two composites materials for induction welding. Eur Phys J Appl Phys Jun. 2002;1(1).
[12] Yarlagadda S, Fink BK, Gillespie JW. Resistive susceptor Design for uniform heating during induction bonding of composites. J Thermoplast Compos Mater Aug. 2016.
[13] Barazanchy D, Van Tooren M. Heating mechanisms in induction welding of thermoplastic composites. J Thermoplast Compos Mater Feb. 2023;36(2):473–92.
[14] Barazanchy D, Pandher J, Van Tooren M. The edge-effect in thermoplastic induction welding. In: Proceedings of AIAA scitech 2021 forum. virtual; Jan. 2021.
[15] Hagenbeek M, Bramon J, Fernandez Villegas I. Controlling the edge effect using a bypass conductor for induction welding of carbon fibre thermoplastic composites. In: Proceedings of 18th European conference on composite materials (ECCM18); 2018. Athens, Grece.
[16] Gouin O, Shaughnessey P, Dubé M, Fernandez Villegas I. Modeling and experimental investigation of induction welding of thermoplastic composites and comparison with other welding processes. J Compos Mater Jan. 2016.
[17] Duhovic M, L'Eplattenier P, Çaldichoury I, Mitschang P, Maier M. Advanced 3D finite element simulation of thermoplastic carbon fiber composite induction welding. In: Proceedings of 16th European conference on composite materials (ECCM16); Jan. 2014. Seville, Spain.
[18] Moser L. Experimental analysis and modeling of susceptorless induction welding of high-performance thermoplastic polymer composites. undefined 2012.
[19] Lionetto F, Pappadà S, Buccoliero G, Maffezzoli A. Finite element modeling of continuous induction welding of thermoplastic matrix composites. Mater Des Apr. 2017;120:212–21.
[20] Hoffman T, Duhovic M, Mang P, Mitschang P. Decoupled electromagnetic simulation of the induction welding process of CFRTP composites. In: Proceedings of 23rd international conference on composites materials (ICCM23); 2023. Belfast, UK.
[21] Grouve W, Vruggink E, Sacchetti F, Akkerman R. Induction heating of UD C/PEKK cross-ply laminates. Procedia Manuf Jan. 2020;47:29–35.
[22] Van den Berg S, Luckabauer M, Wijskamp S, Akkerman R. Determination of the anisotropic electrical conductivity of carbon fabric reinforced composites by the six-probe method. J Thermoplast Compos Mater Nov. 2023;36(11):4257–83.
[23] Teijin Carbon America, Inc. TENAX® continuous filament yarn product data sheet. 2019.
[24] Ji X, Matsuo S, Sottos NR, Cahill DG. Anisotropic thermal and electrical conductivities of individual polyacrylonitrile-based carbon fibers. Carbon Sep. 2022;197:1–9.
[25] Toray Composites Materials America, Inc. T1000G intermediate modulus carbon fiber. 2024.
[26] Toray Composites Materials America, Inc. T700S standard modulus carbon fiber. 2018.
[27] Toray Composites Materials America, Inc. T300 standard modulus carbon fiber. 2018.
[28] Gaier JR, YoderVandenberg Y, Berkebile S, Stueben H, Balagadde F. The electrical and thermal conductivity of woven pristine and intercalated graphite fiber–polymer composites. Carbon Jan. 2003;41(12):2187–93.
[29] Martin RG, Johansson C, Tavares JR, Dubé M. Thermal characterization of thermoplastic composite adherends for induction welding using insulating interlayers. In: Proceedings of 13th Canada-Japan workshop on composites (CJWC13). Québec City: Canada; 2023.
[30] De Wit AJ, Van Hoorn N, Straathof LS, Vankan WJ. Numerical simulation of inductive heating in thermoplastic unidirectional cross-ply laminates. Front in Mater 2023;10.
[31] Barazanchy D, Van Tooren M, Ali M. Microscopic level modeling of induction welding heating mechanisms in thermoplastic composites. J Thermoplast Compos Mater 2021;36(Sep).
[32] Kim H, Yarlagadda S, Shevchenko N, Fink BK, Gillespie J. Development of a numerical model to predict in-plane heat generation patterns during induction processing of carbon fiber-reinforced prepreg stacks. J Compos Mater Aug. 2003;37(16):1461–83.
[33] Castanie B, Bouvet C, Ginot M. Review of composite sandwich structure in aeronautic applications. Compos Part C Open Access Aug. 2020;1:100004.
[34] Barroeta Robles J, Dubé M, Hubert P, Yousefpour A. Repair of thermoplastic composites: an overview. Adv Manuf Polym Compos Sci Apr. 2022;8(2):68–96.
[35] Pegoretti A. Towards sustainable structural composites: a review on the recycling of continuous-fiber-reinforced thermoplastics. Adv Ind Eng Polym Res Apr. 2021;4(2):105–15.
[36] Ageorges C, Ye L. Fusion bonding of polymer composites: from basic mechanisms to process optimization. In: Engineering materials and processes. London: Springer-Verlag; 2002.
[37] Skawinski O, Binetruy C, Krawczak P, Grando J, Bonneau E. All-thermoplastic composite sandwich panels – Part I: manufacturing and improvement of surface quality. Jnl of Sandwich Structures & Materials Sep. 2004;6(5):399–421.
[38] Grünewald J, Parlevliet P, Altstädt V. Definition of process parameters for manufacturing of thermoplastic composite sandwiches – Part B: model verification. J Thermoplast Compos Mater Jun. 2018;31(6):803–19.
[39] Brooks R, Kulandaivel P, Rudd C. Skin consolidation in vacuum moulded thermoplastic composite sandwich beams. In: Proceedings of 8th international conference on sandwich structures (ICSS8); 2008. p. 627–37. Porto, Portugal.
[40] Pappadà S, Rametta R, Passaro A, Lanzilotto L, Maffezzoli A. Processing, mechanical properties, and interfacial bonding of a thermoplastic core-foam/composite-skin sandwich panel. Adv Polym Technol Sep. 2010;29(3):137–223.
[41] Rozant O, Bourban PE, Jae Månson. Manufacturing of three dimensional sandwich parts by direct thermoforming. Compos Part A Appl Sci Manuf Nov. 2001;32(11):1593–601.
[42] Latsuzbaya T, Middendorf P, Voelkle D, Weber C. Fusion bonding of thermoplastic mono-material sandwich structures with honeycomb core. In: Proceedings of SAMPE international conference 2023; 2023. Seattle, WA.
[43] Åkermo M, Aström BT. Modeling compression molding of all-thermoplastic honeycomb core sandwich components. Part B: model verification. Polym Compos 2000;21(2):257–67.
[44] Trende A, Åström BT, Wöginger A, Mayer C, Neitzel M. Modelling of heat transfer in thermoplastic composites manufacturing: double-belt press lamination. Compos Part A Appl Sci Manuf Aug. 1999;30(8):935–43.
[45] Xinyu F, Yubin L, Juan L, Chun Y, Ke L. Modeling of heat conduction in thermoplastic honeycomb core/face sheet fusion bonding. Chin J Aeronaut Dec. 2009;22(6):685–90.
[46] Martin RG, Johansson C, Tavares JR, Dubé M. Manufacturing of thermoplastic composite sandwich panels using induction welding under vacuum. Compos Part A Appl Sci Manuf Jul. 2024;182:108211.
[47] Grünewald J, Parlevliet P, Altstädt V. Definition of process parameters for manufacturing of thermoplastic composite sandwiches – Part A: modelling. J Thermoplast Compos Mater Sep. 2017.
[48] Smiley AJ, Halbritter A, Cogswell F, Meakin PJ. Dual polymer bonding of thermoplastic composite structures. Polym Eng Sci May 1989;31(7):526–32.
[49] Cogswell FN, Meakin PJ, Smiley AJ, Harvey MT, Booth C. Thermoplastic interlayer bonding of aromatic polymer composites. Compos Manuf 1991;2(2):86–91.
[50] Hsiao BS, Sauer BB. Glass transition, crystallization, and morphology relationships in miscible poly(aryl ether ketones) and poly(ether imide) blends. J Polym Sci, Part B: Polym Phys 1993;31(8):901–15.
[51] Teijin Carbon America, Inc. Tenax®-E TPUD PEEK-2-34-HTS45 P12 12K-UD-145 product data sheet. 2020.
[52] Martin RG, Figueiredo M, Johansson C, Tavares JR, Dubé M. Hysteresis losses magnetic susceptor heating rate characterization. In: Proceedings of SAMPE international conference 2023. Seattle, WA; 2023.
[53] Ageorges C, Ye L, Mai YW, Hou M. Characteristics of resistance welding of lap shear coupons. Part I: heat transfer. Compos Part A Appl Sci Manuf Aug. 1998;29(8):899–909.
[54] Holmes ST, Gillespie JW. Thermal analysis for resistance welding of large-scale thermoplastic composite joints. J Reinforc Plast Compos Jun. 1993;12(6):723–36.
[55] Widagdo D, Kuswoyo A, Nurpratama TO, Hadi BK. Experimental flatwise tensile strength dataset of carbon fibre reinforced plastic sandwich panels with different core material preparations. Data Brief Feb. 2020;28:105055.
[56] Hegde SR, Hojjati M. Effect of core and facesheet thickness on mechanical property of composite sandwich structures subjected to thermal fatigue. Int J Fatig Oct. 2019;127:16–24.
[57] Butukuri RR, Bheemreddy V, Chandrashekhara K, Berkel TR, Rupel K. Evaluation of skin-core adhesion bond of out-of-autoclave honeycomb sandwich structures. J Reinforc Plast Compos Mar. 2012;31:331–9.